Groove instability in cellular solidification

Massimo Conti* and Umberto Marini Bettolo Marconi
Dipartimento di Matematica e Fisica and Istituto Nazionale di Fisica della Materia, Università di Camerino, Via Madonna delle Carceri, 62032, Camerino, Italy

(Received 10 May 2000; revised manuscript received 12 September 2000; published 18 December 2000)

We simulate in two dimensions the cellular solidification of a binary alloy, to focus on the emergence of a secondary instability consisting in the periodic detachment of liquid droplets from the bottom of the intercellular liquid grooves. This phenomenon, observed in the solidification of thin samples, was previously interpreted in terms of an instability of the liquid-jet type; as it should occur only in three-dimensional systems, it was argued that even for thin samples the grooves have a tubelike structure. Recently the droplets detachment has been evidenced also in a two-dimensional simulation, so that a different interpretation should be given. We show that the phenomenon arises as the result of diffusional and capillary effects driven by the strong curvature of the solid–liquid interface. The dependence of the emission frequency and the droplets radius on the growth velocity is also studied.

DOI: 10.1103/PhysRevE.63.011502 PACS number(s): 64.70.Dv, 81.15.Lm, 81.30.Bx, 68.35.Md

Directional solidification experiments conducted on thin samples of binary alloys, in the cellular growth regime, displayed the emergence of a secondary instability consisting in the periodic detachment of liquid droplets at the bottom of the intercellular liquid grooves [1]. These droplets, already reported in the literature by Sato and Ohira for an Al–Cu alloy [2], are strongly enriched in solute and survive for some time as they are advected back into the solid. The droplets diameter D was found in the range $0.1<D/\lambda<0.2$, λ being the spacing between the cells tips, and the spatial periodicity L_p is of the order of $\lambda/2$. The interpretation of the phenomenon in terms of a Rayleigh-type instability led Brattkus [3] to conclude that even for thin samples the grooves have a three-dimensional structure; on the other side, numerical studies conducted in two dimensions [4–6] showed the formation of a bulge at the bottom of the grooves, but the pinch-off which should be responsible of the droplets detachment had not been observed. Recently the droplets formation has been evidenced also in a two-dimensional simulation [7], opening a new perspective for the understanding of this instability.

In the present study we use the phase-field model [8–11] to simulate the directional solidification of a binary alloy. The results will show that the emission of solute-enriched liquid droplets, observed in two dimensions, is due to diffusional and capillary effects inside the liquid grooves. We found that at fixed values of the thermal gradient the drops radius decreases with increasing the emission frequency, in agreement with the experimental data [1]; the emission frequency is in turn an increasing function of the pulling speed. The system is an ideal binary solution with constituents A (solvent) and B (solute). Initially a solid ($x<x_0$) and a liquid ($x>x_0$) region are separated by an interface at temperature $\overline{T_I}$; the solute concentration c is fixed on the solidus line at $\overline{T_I}$. Then the temperature field $T(x)$, characterized by a positive uniform gradient G, is pulled towards the positive x direction at constant velocity V, and the solidification front follows the advancing isotherms. With this arrangement we neglect the latent heat released at the growing interface. At large growth rates this approximation ceases to be satisfactory, however we believe that the relevant features of the solidification process are still preserved. The problem that will be treated is scaling lengths to the reference length $\xi=2.1\times10^{-4}$ cm and time to ξ^2/D_l, D_l being the solute diffusivity in the liquid phase. Allowing for anisotropy of the surface tension, the field equations become

$$\phi_t=[(1-c)m^A+c\,m^B]\{\nabla[\eta^2(\theta)\nabla\phi]+[\eta(\theta)\eta'(\theta)\phi_x]_y-[\eta(\theta)\eta'(\theta)\phi_y]_x+(1-c)Q^A(T,\phi)+cQ^B(T,\phi)\}, \tag{1}$$

$$c_t=-\nabla\{c(1-c)\lambda(\phi)[H^A(\phi,T)-H^B(\phi,T)]\nabla\phi+c(1-c)\lambda(\phi)\Gamma(\phi,T)\nabla T-\lambda(\phi)\nabla c\}, \tag{2}$$

$$T_t=-VG. \tag{3}$$

In the above equations ϕ is an order parameter assuming the values $\phi=0$ in the bulk solid and $\phi=1$ in the liquid. The functions $H^{A,B}(\phi,T)$, $Q^{A,B}(\phi,T)$, and $\Gamma(\phi,T)$ are defined as

$$H^{A,B}(\phi,T)=W^{A,B}g'(\phi)-L^{A,B}\frac{v_m}{R}p'(\phi)\frac{T-T^{A,B}}{TT^{A,B}}, \tag{4}$$

$$Q^{A,B}(\phi,T)=-\frac{\xi^2}{(h^{A,B})^2}g'(\phi)+\frac{1}{6\sqrt{2}}\frac{\xi^2L^{A,B}}{\sigma^{A,B}h^{A,B}}\frac{T-T^{A,B}}{\overline{T_I}}p'(\phi), \tag{5}$$

$$\Gamma(\phi,T)=-\frac{v_m}{R}\frac{p(\phi)}{T^2}(L^A-L^B), \tag{6}$$

*Electronic address: conti@campus.unicam.it

TABLE I. Material parameters for the Ni–Cu alloy.

Parameter	Nickel	Copper
T_m (K)	1728	1358
L (J/cm^3)	2350	1728
v_m (cm^3/mole)[a]	7.0	7.8
σ (J/cm^2)	3.7×10^{-5}	2.8×10^{-5}
D_l (cm^2/s)	10^{-5}	10^{-5}

[a]An average value of 7.4 will be taken.

where $g(\phi)=\phi^2(1-\phi)^2/4$ is a symmetric double well potential with equal minima at $\phi=0$ and $\phi=1$; the function $p(\phi)$, defined as $p(\phi)=\phi^3(10-15\phi+6\phi^2)$ enforces the condition that the bulk solid and liquid are described by $\phi=0$ and $\phi=1$, respectively, for every value of temperature. $L^{A,B}$ and $T^{A,B}$ represent the latent heat per unit volume and the melting temperature of the pure components A or B; R is the gas constant and v_m is the molar volume. In Eq. (5) $\sigma^{A,B}$, $h^{A,B}$ indicate the surface tension and the interface thickness of the components A and B, respectively. The function $\lambda(\phi)$, defined as $\lambda(\phi)=D_s/D_l+p(\phi)(1-D_s/D_l)$ describes the smooth transition of the bulk solute diffusivity from D_s (in the solid) to D_l (in the liquid). The model parameters $m^{A,B}$, $W^{A,B}$ depend on the physical properties of the alloy components as [10] $m^{A,B}=(\beta^{A,B}\sigma^{A,B}T^{A,B})/(D_lL^{A,B})$, $W^{A,B}=(12v_m\sigma^{A,B})/(\sqrt{2}RT^{A,B}h^{A,B})$, where $\beta^{A,B}$ is the kinetic undercooling coefficient of pure A or B. Equation (1) accounts for the anisotropy of surface energy: θ is the angle between the normal to the interface and a fixed direction (the x axis in our calculations) and the function $\eta(\theta)=(1+0.01\cos4\theta)$ enforces a fourfold symmetry [12]. To fix the model parameters we referred to the physical properties of a nickel (solvent) and copper (solute) binary alloy, which are summarized in Table I; the solute diffusivity in the solid phase was estimated as $D_s=10^{-6}\times D_l$. Due to limitations of the computational resources, the value selected for the interface thickness ($h^{A,B}=4.2\times10^{-6}$ cm) is about 10 times larger than actual values; moreover we chose $\beta^A=0.511$ cm s^{-1} K^{-1} and $\beta^B=0.641$ cm s^{-1} K^{-1}, values much smaller than the actual best estimates. These approximations determine a shift of the dynamical $T_I(v)$ curve towards lower values of the growth velocity, but do not affect the interplay between the diffusional and capillary effects at the basis of the process evolution.

Equations (1)–(3) have been solved on the computational domain $0\leqslant x\leqslant x_m, 0\leqslant y\leqslant y_m$ with $x_m=6.40$ and $y_m=0.48$. An explicit Euler integration scheme was employed to advance the solution forward in time and second order central differences were used to discretize the Laplace operator. To ensure an accurate resolution of both the phase and the concentration profiles (and mesh independent results) the grid spacing was selected as $\Delta x=\Delta y=8\times10^{-3}$; details of the numerical method are reported in [13].

The initial concentration of the alloy was set to $c_\infty=0.4$ (atomic fraction), on the solidus line at $\overline{T_I}=1573$ K; then the initial temperature profile defined as $T(x,0)=\overline{T_I}+G(x-x_0)$ was pulled towards the positive x direction, starting solidification. After the process reached the stationary regime, to activate the two-dimensional dynamics a periodic corrugation $x_f(y,t^*)=x^*+0.1\sin(4\pi y/y_m)$ was forced at time t^* on the planar interface located at $x_f(y,t^*)=x^*$. Here and in the following, except for temperatures, all the results will be presented in nondimensional units; for the reader's commodity we recall that the length scale is fixed at $\xi=2.1\times10^{-4}$ cm, and the resulting time and velocity scales are 4.41×10^{-3} s and 4.76×10^{-2} cm/s, respectively; the thermal gradient G is given in temperature units, as it is referred to a nondimensional length.

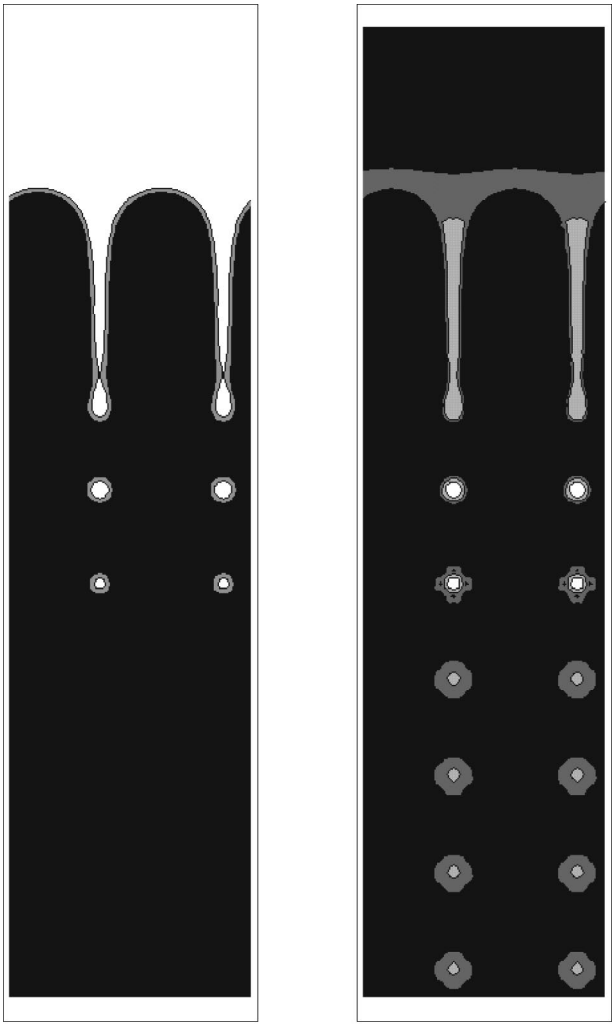

FIG. 1. Contour plots of the phase (left) and solute (right) fields for cellular solidification at $t=0.24$ for $V=12$ and $G=8$ K. Only a portion ($1.92\leqslant x\leqslant3.84$) of the computational domain is represented. In order of decreasing darkness we have three zones for the phase field: $\phi\leqslant0.33$ (solid), $0.33<\phi\leqslant0.66$, and $\phi>0.66$ and four zones for the concentration field: $c\leqslant0.425$, $0.425<c\leqslant0.450$, $0.450<c\leqslant0.475$, and $c>0.475$ (atomic fractions).

In the region of the G,V plane we explored two cells were allowed to grow into the liquid, though we observed also the planar growth limit (at low pulling velocities) and the tip splitting and the subsequent formation of four cells for large growth rates. The effects of the groove instability are displayed in Fig. 1, where the cellular configuration is shown

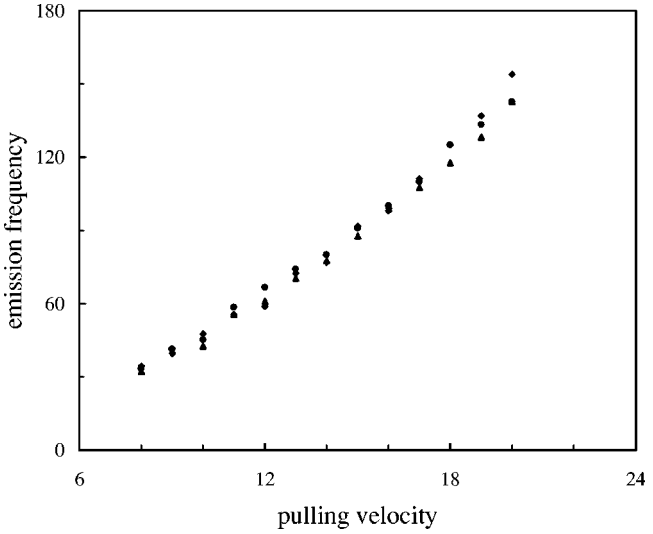

FIG. 2. The emission frequency of the droplets versus the pulling velocity for $G=4$ K (diamonds), $G=8$ K (solid circles), and $G=12$ K (triangles).

for $G=8$ K and $V=12$. In the same graph both the phase (left-hand side) and the solute fields (right-hand side) are represented. It is clearly recognizable that the trail of droplets left behind the advancing solidification front, on the axes of the liquid grooves. The spacing between the cells tips is $\lambda=0.240$; the droplets spatial periodicity is $L_p=0.192$ and the time emission periodicity is $\tau=1.6\times10^{-2}$, that is $L_p=V\tau$. The droplets diameter, immediately after the emission and the subsequent sphericization, is $D=4.6\times10^{-2}$. Rescaling the pattern configuration to the intercellular spacing we have $L_p/\lambda=0.80$ and $D/\lambda=0.19$, in good agreement with the experimental data. The snapshot has been taken just at the moment in which we can observe the pinch-off of the liquid bulges. Notice that the droplets frozen in the solid phase

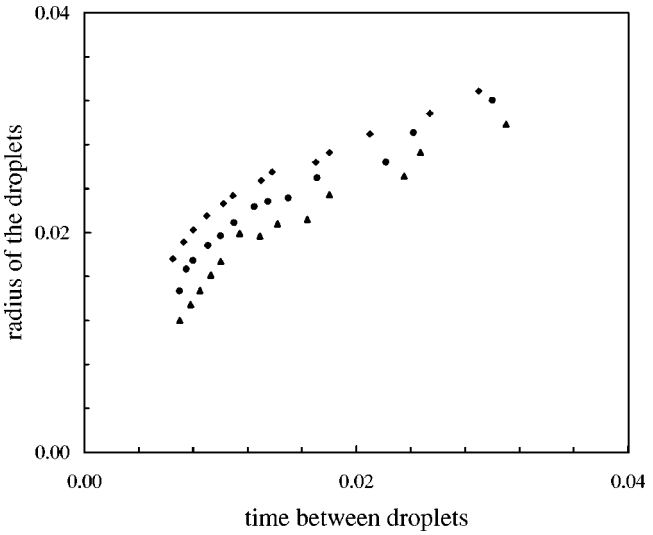

FIG. 3. The radius of the droplets increases with increasing the emission time. Each set of data refers to a different value of the thermal gradient G: $G=4$ K (diamonds), $G=8$ K (solid circles), and $G=12$ K (triangles).

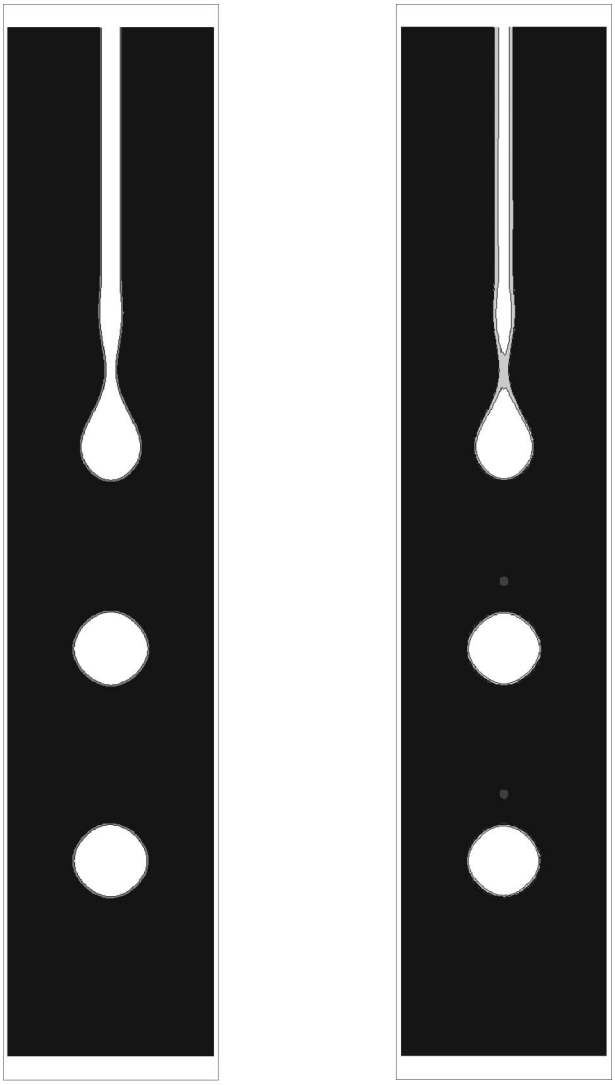

FIG. 4. Contour plots of the phase (left-hand side) and solute (right-hand side) fields for the shrinking dynamics of the planar strip, at $t=6$. The initial length and width of the strip are $L_0=9.12$ and $W=8.80\times10^{-2}$. In order of decreasing darkness we have three zones for the phase field: $\phi\leqslant0.33$ (solid), $0.33<\phi\leqslant0.66$, and $\phi>0.66$, and six zones for the concentration field: $c\leqslant0.405$, $0.405<c\leqslant0.418$, $0.418<c\leqslant0.431$, $0.431<c\leqslant0.444$, $0.444<c\leqslant0.457$, and $c>0.457$ (atomic fractions).

correspond to highly solute-enriched regions; for this reason they survive for some time after being advected into the solid phase. We found that the solidification front at the bottom of the groove follows a cyclic dynamics, retarding in respect to the thermal field for the most part of the cycle, during the bulge formation. When the pinch-off of the bulge occurs the solid-liquid interface becomes cusp-shaped (see Fig. 1) and the (negative) curvature becomes locally infinite. Due to the Gibbs-Thomson effect the driving force for solidification becomes also infinite: the bottom of the groove is suddenly advanced and the interface temperature is raised. It is reasonable to argue that the observed pinch-off occurs when the neck of the bulge is cooled below a certain level. In this case the emission frequency $f_e=1/\tau$ should increase with increas-

ing the pulling velocity. This suggestion is confirmed in Fig. 2 where we see that f_e is essentially determined by the isotherm velocity, while the thermal gradient has a minor effect on the timing of the process. The experiments of Kurowski *et al.* [1] indicated a tendency to emit smaller droplets at larger frequencies but, due to the strong scattering of the data (see Fig. 4 of that reference) this point was not definitely clarified. Figure 3 shows that the droplets radius is a decreasing function of the emission frequency; the three sets of data correspond to different values of the thermal gradient. This result can be explained observing that the emission frequency is controlled by the pulling velocity; on the other side, the growth rate of the bulge depends on the local shape of the liquid groove which, in turn, is strongly affected by the thermal gradient G. As V (and f_e) increase the bulge has little time to develop before the detachment and the resulting droplets are small. The droplets emission is not always observed, and disappears for sufficiently high values of the thermal gradient or of the pulling velocity. It is reasonable to argue that in these cases the bulge has no time to develop and to detach before that freezing occurs.

The details of the solidification dynamics, during the bulge formation and detachment, are not accessible to analytic calculation especially in the strong nonlinear regime characteristic of deep cells. However, to get some insight into this interesting behavior we observe that it presents strong analogies with a different but simpler phenomenon. We start observing that the intercellular groove can be considered as a thin liquid strip, in which the solute concentration is not far from equilibrium, surrounded by the walls of the adjacent solid cells. The shrinking of such a strip, of rectangular shape and large aspect ratio, was addressed [14] in the context of a phase separation problem (model B). We now are going to extend these results to the formally nonconserved dynamics (model C) of a solidification process; however previous studies [15] demonstrated that in the curvature driven coarsening of liquid domains (the problem in which we are interested) to a good extent of accuracy the order parameter can be considered as conserved. The liquid strip, of initial length L_0 and width $W \ll L_0$, is prepared along the x axis, in thermal and chemical equilibrium with the surrounding solid phase. In a static thermal field due to the interface curvature (largest and negative near the strip ends), the strip shrinks along its main axis assuming the shape of a ''dumbbell.'' If we assume that the bulges at the dumbbell ends can be chacterized by a single time-dependent length scale $R(t)$, it is found that the length reduction $l(t)$ of the strip in the process of its shrinking scales as $l(t) \sim W^{-1/2} t^{1/2}$ while the radius of the bulges increases as $R(t) \sim W^{1/4} t^{1/4}$ [14]. The matching of the bulges to the planar part of the strip is characterized by positive curvature and acts as a sink of solute from both the bulge and the adjacent planar region; as a consequence the latter is progressively solidified, acquiring the characteristic shape of a bottleneck which is throttled until the bulge is detached from the strip. If we assume that detachment occurs when an area of the order of W^2 is solidified, dimensional analysis shows that the time required scales as W^3. The effects of the shrinking dynamics are displayed in Fig. 4, where both the phase (left-hand side) and the solute fields (right-hand side) are represented; the process has been simulated through the same governing equations (and the same physical parameters) as for cellular solidification, but assuming a static thermal field. The strip width and initial length are $W = 8.80 \times 10^{-2}$ and $L_0 = 9.12$, respectively. Due to the symmetry of the problem, only one-half of the strip is shown in the figure. We can observe the trail of (solute enriched) liquid bubbles which result from the fragmentation of the liquid strip. The spatial periodicity is $L_p = 1.08$ and the time between droplets is $\tau = 1.99$. The scaling of the emission time with the strip width has been checked over less than a decade, as the numerical cost of the simulations increases dramatically with W; however, we observed that the guess $\tau \sim W^3$ is reasonable, as the best fit for the numerical data is $\tau \sim W^{2.86}$.

In summary, a jet-type instability, driven by both diffusional and capillary effects, can be observed also in two dimensions for the isothermal dynamics of a liquid strip surrounded by its solid phase. The same physical picture is ultimately at the origin of the groove instability in cellular solidification. In the latter case the droplets emission should be observed when the velocity of the thermal field is slow enough to allow the bulge formation and detachment. Rescaling the solidification pattern to the intercellular spacing, both the droplets diameter and periodicity result in good agreement with the experimental data.

[1] P. Kurowski, S. de Cheveignè, G. Faivre, and C. Guthmann, J. Phys. (France) **50**, 3007 (1990).
[2] T. Sato and G. Ohira, Trans. Jpn. Inst. Met. **12**, 285 (1971).
[3] K. Brattkus, J. Phys. (France) **50**, 2999 (1990).
[4] D.A. Kessler and H. Levine, Phys. Rev. A **39**, 3208 (1989).
[5] L.H. Ungar and R.A. Brown, Phys. Rev. B **29**, 1367 (1984).
[6] Y. Saito, C. Misbah, and H. Müller-Krumbhaar, Phys. Rev. Lett. **63**, 2377 (1989).
[7] W.J. Boettinger and J.A. Warren, J. Cryst. Growth **200**, 583 (1999).
[8] G. Caginalp and J. Jones, Ann. Phys. (N.Y.) **237**, 66 (1995).
[9] A.A. Wheeler, W.J. Boettinger, and G.B. McFadden, Phys. Rev. A **45**, 7424 (1992).
[10] J.A. Warren and W.J. Boettinger, Acta Metall. Mater. **43**, 689 (1995).
[11] Z. Bi and R.F. Sekerka, Physica A **261**, 95 (1998).
[12] G.B. McFadden, A.A. Wheeler, R.J. Braun, and S.R. Coriell, Phys. Rev. E **48**, 2016 (1993).
[13] M. Conti, Phys. Rev. E **58**, 6101 (1998).
[14] M. Conti, B. Meerson, and P. Sasorov, Phys. Rev. Lett. **80**, 4693 (1998).
[15] M. Conti, F. Marinozzi, and U. Marini Bettolo Marconi, Europhys. Lett. **36**, 431 (1996).